SUPPORTING INFORMATION

Structural, Magnetic and Spectral Properties of Tetrahedral Cobalt(II) Silanethiolates: Variety of Structures and Manifestation of Field-Induced Slow Magnetic Relaxation

Daria Kowalkowska-Zedler,[†] Anna Dołęga,[†] Natalia Nedelko,[‡] Renata Łyszczek,[§] Pavlo Aleshkevych,[‡] Iraida Demchenko,[£] Justyna Łuczak,[¥] Anna Ślawska-Waniewska,[‡] and Agnieszka Pladzyk*[†]*

† Department of Inorganic Chemistry, Chemical Faculty, Gdańsk University of Technology, Narutowicza Str. 11/12, 80-233 Gdańsk, Poland
‡ Institute of Physics, Polish Academy of Sciences, Aleja Lotników 32/46, 02-668 Warsaw, Poland
§ Department of Coordination and General Chemistry, Maria Curie-Skłodowska University, M.C. Skłodowska Sq. 2, 20-031 Lublin, Poland
£ Department of Chemistry, University of Warsaw, Pasteur Str 1, 02-093 Warsaw, Poland
¥ Department of Chemical Technology, Chemical Faculty, Gdańsk University of Technology, Narutowicza Str. 11/12, 80-233 Gdańsk, Poland

To whom correspondence should be addressed.
Email: agnieszka.pladzyk@pg.edu.pl
slaws@ifpan.edu.pl

Supplementary Index

1. STRUCTURAL DATA

Table S1. Crystallographic data and structure refinement results for complexes **1**-**5**

Complexes	**1**	**2**	**3**	**4**	**5**
Empirical formula	$C_{103}H_{206}N_{12}Co_3O_{21}S_6Si_6$	$C_{35.5}H_{66}N_4CoO_{7.5}S_2Si_2$	$C_{36}H_{74}N_4CoO_8S_2Si_2$	$C_{60}H_{124}N_4Co_2O_{12}S_4Si_4$	$C_{30}H_{62}N_2CoO_6S_2Si_2$
M_r /g mol^{-1}	2486.48	848.15	870.22	1452.08	726.04
T (K)	120	120	120	120	120
Wavelength /Å	0.71073 (Mo K_α)	0.71073 (Mo K_α)	0.71073 (Mo K_α)	0.71073 (Mo K_α)	0.71073 (Mo K_α)
Crystal system	triclinic	triclinic	triclinic	triclinic	orthorhombic
Space group	*P*-1	*P*-1	*P*-1	*P*-1	$Pca2_1$
a (Å)	15.779(6)	9.556(9)	9.825(3)	9.182(5)	27.991(3)
b (Å)	21.493(5)	13.484(13)	15.238(4)	14.081(13)	9.623(3)
c (Å)	22.043(6)	20.611(14)	18.819(5)	16.395(7)	16.419(3)
α (°)	70.174(19)	99.29(5)	108.65(2)	104.97(5)	90
β (°)	79.49(3)	101.10(6)	96.17(2)	94.60(4)	90
γ (°)	82.11(3)	108.21(6)	108.46(2)	99.97(6)	90
V (Å^3)	6891(4)	2405(3)	2462.9(12)	1999(2)	4422.6(17)
Z	2	2	2	1	4
Crystal size (mm)	0.253×0.243×0.233	0.068×0.171×0.345	0.28×0.255×0.239	0.345×0.171×0.068	0.265×0.149×0.071
D_{calc} (Mg m^{-3})	1.198	1.171	1.173	1.206	1.090
θ range (°)	1.943 to 25.999	2.452 to 25.997	2.86 to 28.86	2.47 to 25.999	2.116 to 25.999
Reflections collected/unique	53380 / 26627	18030 / 9265	33508 / 9265	14827 / 7741	30977/8288
R_{int}	0.0469	0.0453	0.0372	0.0453	0.1237
μ (mm^{-1})	0.561	0.538	0.527	0.631	0.571
Data / restraints / parameters	26627 / 5 / 1431	9265 / 6 / 503	9265 / 0 / 522	7741 / 0 / 414	8288 / 1 / 324
GOF on F^2	0.85	1.054	1.038	1.043	1.037
Final *R* indices					
R_1, wR_2 [$I > 2\sigma(I)$]	0.0449, 0.0949	0.0422, 0.1035	0.0361, 0.0899	0.0422, 0.1035	0.0942, 0.2155
R_1, wR_2 (all data)	0.0827, 0.1048	0.0588, 0.1117	0.0511, 0.0955	0.0588, 0.1117	0.1339, 0.2413
Largest diff. peak and hole (eÅ^{-3})	1.036 and -0.448	0.897 and -0.347	0.511 and -0.291	0.897 and -0.347	0.983 and -0.481
CCDC number	1894270	1894273	1894274	1894275	1894276

Table S2. Selected bond distances (Å) for complexes **1**-**5**

	1	**2**	**3**	**4**	**5**
Bond length [Å]					
Co(1)-N(1)	2.073(3)	2.066(3)	2.0208(16)	2.041(2)	2.048(8)[ii]
Co(1)-N(2)				2.060(2)[i]	
Co(1)-N(3)	2.041(2)	2.041(4)	2.0057(15)		
Co(2)-N(5)	2.061(3)				2.029(8)
Co(2)-N(7)	2.048(2)				
Co(3)-N(9)	2.038(2)				
Co(3)-N(11)	2.057(3)				
Co(1)-S(1)	2.3024(11)	2.294(3)	2.3101(10)	2.2773(16)	2.291(2)
Co(1)-S(2)	2.2759(10)	2.2956(18)	3.3127(7)	2.270(2)	2.310(3)
Co(2)-S(3)	2.2922(10)				
Co(2)-S(4)	2.3044(10)				
Co(3)-S(5)	2.2909(9)				
Co(3)-S(6)	2.3126(10)				
Si(1)-S(1)	2.0999(13)	2.0883(18)	2.0843(8)	2.070(2)	2.068(3)
Si(2)-S(2)	2.0929(13)	2.079(3)	2.0888(9)	2.0827(16)	2.073(3)
Si(3)-S(3)	2.0923(12)				
Si(4)-S(4)	2.1007(13)				
Si(5)-S(5)	2.0979(12)				
Si(6)-S(6)	2.0989(13)				
Si(1)-O(1)	1.624(2)	1.629(4)	1.6324(13)	1.631(2)	1.634(8)
Si(1)-O(2)	1.616(2)	1.619(3)	1.6244(13)	1.626(2)	1.597(9)
Si(1)-O(3)	1.6283(18)	1.628(4)	1.6321(14)	1.6507(19)	1.620(6)
Si(2)-O(4)	1.625(2)	1.625(3)	1.6219(14)	1.627(2)	1.648(7)
Si(2)-O(5)	1.627(2)	1.621(3)	1.6306(15)	1.633(2)	1.625(9)
Si(2)-O(6)	1.638(2)	1.625(3)	1.6286(13)	1.647(2)	1.622(9)
Si(3)-O(7)	1.631(2)				
Si(3)-O(8)	1.6248(19)				
Si(3)-O(9)	1.626(2)				
Si(4)-O(10)	1.6186(19)				
Si(4)-O(11)	1.625(2)				
Si(4)-O(12)	1.6290(18)				
Si(5)-O(13)	1.6230(19)				
Si(5)-O(14)	1.625(2)				
Si(5)-O(15)	1.628(2)				
Si(6)-O(16)	1.6187(19)				
Si(6)-O(17)	1.6330(18)				
Si(6)-O(18)	1.631(2)				

Symmetry code(s): (i) –x+1, -y+1, -z+1; (ii) –x+1, -y+1, z-1/2;

Table S3. Selected bond angles (°) for complexes **1**-**5**

Bond angles [deg]	**1**	**2**	**3**	**4**	**5**
N(1)-Co(1)-N(2)				106.57(9)[i]	
N(1)-Co(1)-N(3)	104.87(11)	108.06(14)	115.10(6)		
N(1)-Co(1)-N(5)					110.7(3)[ii]
N(5)-Co(2)-N(7)	111.55(10)				
N(9)-Co(3)-N(11)	106.04(10)				
N(1)-Co(1)-S(1)	107.05(8)	95.93(12)	109.52(5)	110.15(8)	113.3(2)[ii]
N(2)-Co(1)-S(1)				109.09(8)[i]	

N(3)-Co(1)-S(1)	111.22(8)	111.84(12)	111.61(5)		
N(5)-Co(1)-S(1)					108.5(2)
N(1)-Co(1)-S(2)	112.59(7)	113.38(11)	108.27(5)	105.10(8)	101.7(2)[i]
N(2)-Co(1)-S(2)				107.16(9)[i]	
N(3)-Co(1)-S(2)	110.42(8)	113.04(12)	111.41(5)		
N(5)-Co(1)-S(2)					112.7(2)
N(5)-Co(2)-S(3)	112.17(7)				
N(7)-Co(2)-S(3)	109.68(7)				
N(5)-Co(2)-S(4)	99.83(7)				
N(7)-Co(2)-S(4)	110.19(7)				
N(9)-Co(3)-S(5)	111.67(8)				
N(11)-Co(3)-S(5)	113.91(7)				
N(9)-Co(3)-S(6)	111.19(8)				
N(11)-Co(3)-S(6)	103.31(8)				
S(1)-Co(1)-S(2)	110.54(4)	113.31(8)	99.82(3)	118.14(6)	109.80(9)
S(3)-Co(2)-S(4)	113.14(4)				
S(5)-Co(3)-S(6)	110.37(4)				
Si(1)-S(1)-Co(1)	107.41(5)	107.45(8)	110.15(3)	109.60(6)	106.81(12)
Si(2)-S(2)-Co(1)	114.06(5)	105.84(8)	112.95(3)	109.63(7)	105.48(13)
Si(3)-S(3)-Co(2)	104.58(4)				
Si(4)-S(4)-Co(2)	107.89(4)				
Si(5)-S(5)-Co(3)	105.77(4)				
Si(6)-S(6)-Co(3)	106.43(4)				

Symmetry code(s): (i) –x+1, -y+1, -z+1; (ii) –x+1, -y+1, z-1/2;

Table S4. Hydrogen bonds parameters for complexes **1**-**5**

	D—H···A	D—H [Å]	H···A [Å]	D···A [Å]	∠ DHA [°]
1	N8—H8E···O19	0.86	2.2	3.013(3)	158.3
	N12—H12D···O19	0.86	2.8	3.473(4)	135.7
	N12—H12E···O21	0.86	2.21	3.056(4)	164.6
	O20—H20G···S4	0.85	2.68	3.505(3)	163.6
	O19—H19G···S6	0.896(5)	2.599(5)	3.331(2)	139.4(8)
	O19—H19H···S5	0.895(5)	2.597(5)	3.315(2)	137.8(8)
2	N2—H2B···S1[i]	0.86	2.64	3.498(5)	171.4
	N4—H4D···S1[ii]	0.87	2.97	3.714(5)	144.2
	N4—H4E···O8B	0.87	2.44	3.182(13)	143.4
3	O7—H7···S2	0.74(3)	2.59(3)	3.300(2)	161(3)
	O8—H8···O7	0.71(2)	2.09(2)	2.797(2)	170(3)
	N2—H2A···S1[i]	0.91(2)	2.56(2)	3.4023(19)	153.7(18)
	N2—H2B···S2[i]	0.77(2)	2.74(2)	3.374(2)	142(2)
	N4—H4A···O7[ii]	0.82(3)	2.44(3)	3.091(3)	137(2)
	N4—H4B···O8[iii]	0.83(3)	2.16(3)	2.944(3)	159(2)
4	N2—H2E···O3[iiii]	0.85(3)	2.17(3)	2.978(4)	158(3)
	N2—H2D···O6[iiii]	0.80(3)	2.18(3)	2.936(4)	157(3)
5	N1—H1A···O5[iiiii]	0.89	2.26	3.016(10)	143.2

Symmetry code(s): (i) –x+2, -y+1, -z+1; (ii) x-1, y, z; (iii) –x+2, -y+2, -z+2; (iiii) –x+1, -y+1, -z+1; (iiiii) –x+1, -y+1, z+1/2;

Table S5. The values of torsion angles in **4** and **5**.

compound 4		**compound 5**	
angle	[°]	angle	[°]
S1-Co1-S2-Si2	**-82**	S1-Co1-S2-Si2	**177.8**
S2-Co1-S1-Si1	**164.1**	S2-Co1-S1-Si1	**152.7**
N2-Co1-N1-C29	-76.5	N1-Co1-N5-C25	-70
N2-Co1-N1-C25	99.5	N1-Co1-N5-C29	113
N1-Co1-N2-C30	**-21.1**	**N5-Co1-N1-C30**	**168.6**
N1-Co1-N2-H2E	**100**	**N5-Co1-N1-H1A**	**-70.6**
N1-Co1-N2-H2D	**-145**	**N5-Co1-N1-H1B**	**47.54**

2. SPECTRAL DATA

Table S6. UV-Vis reflectance spectra of **1-5**.

	UV λ_{max} [nm]	Vis λ_{max} [nm]
1	233; 302; 364sh	600; 643; 673
2	242; 311; 361sh	606; 640; 664
3	270; 325sh	588; 618; 669
4	260; 292; 336(362sh)	590; 634; 676
5	255; 295; 336sh	604; 654; 679

3. MAGNETIC DATA

Table S7. The parameters of Cole-Cole fitting of **2** and **4** under different *dc* magnetic fields at 2 K. Cole-Cole plots were fitted using the formulas describing χ' and χ'' as a function of frequency:[1]

$$\chi'(\omega) = \chi_S + \frac{\chi_{TS}\left(1+(\omega\tau)^{1-\alpha}\sin(\pi\alpha/2)\right)}{1+2(\omega\tau)^{1-\alpha}\sin(\pi\alpha/2)+(\omega\tau)^{2(1-\alpha)}} \text{ and } \quad \chi''(\omega) = \frac{\chi_{TS}(\omega\tau)^{1-\alpha}\cos(\pi\alpha/2)}{1+2(\omega\tau)^{1-\alpha}\sin(\pi\alpha/2)+(\omega\tau)^{2(1-\alpha)}},$$

where, $\omega = 2\pi\nu$ and $\chi_{TS} = \chi_T - \chi_S$, ($\chi_T$ and χ_S are the isothermal and adiabatic susceptibilities, respectively), τ – relaxation time and α – a variable representing the distribution of relaxation times.

[1] K. S. Cole, R. H. Cole, *J. Chem. Phys.,* 1941, **9**, 341.

2					**4**				
H kOe	τ ms	χ_{TS}	χ_{SC}	α	*H* kOe	τ ms	χ_{TS}	χ_{SC}	α
0.1	0.030	0.278	0.490	0.047	**0.1**	0.025	0.253	0.238	0.180
0.4	0.064	0.594	0.170	0.068	**0.4**	0.054	0.368	0.128	0.144
0.7	0.070	0.630	0.115	0.076	**0.7**	0.066	0.324	0.173	0.165

1	0.070	0.619	0.095	0.084	**1**	0.085	0.368	0.124	0.114
1.5	0.065	0.571	0.082	0.099	**1.5**	0.086	0.389	0.100	0.117
2	0.059	0.510	0.075	0.119	**2**	0.093	0.381	0.100	0.135
3	0.044	0.393	0.063	0.161	**3**	0.099	0.306	0.164	0.187
4	0.032	0.294	0.061	0.192	**4**	0.091	0.189	0.255	0.238
6	0.014	0.191	0.045	0.292	**6**	0.190	0.198	0.188	0.215
					8	0.207	0.178	0.127	0.175
					10	0.124	0.129	0.099	0.137
					15	0.027	0.051	0.074	0.177

4. SUPPORTING FIGURES

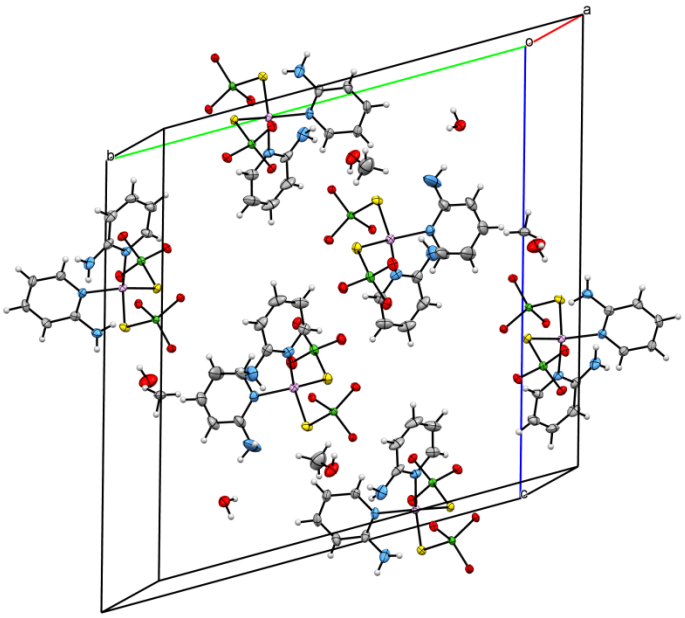

Fig. S1 The crystal packing of **1** along *b* axis. H atoms and *t*Bu groups omitted for clarity (S-yellow, O-red, N-blue, Si-green, Co-pink, C – grey, H-white).

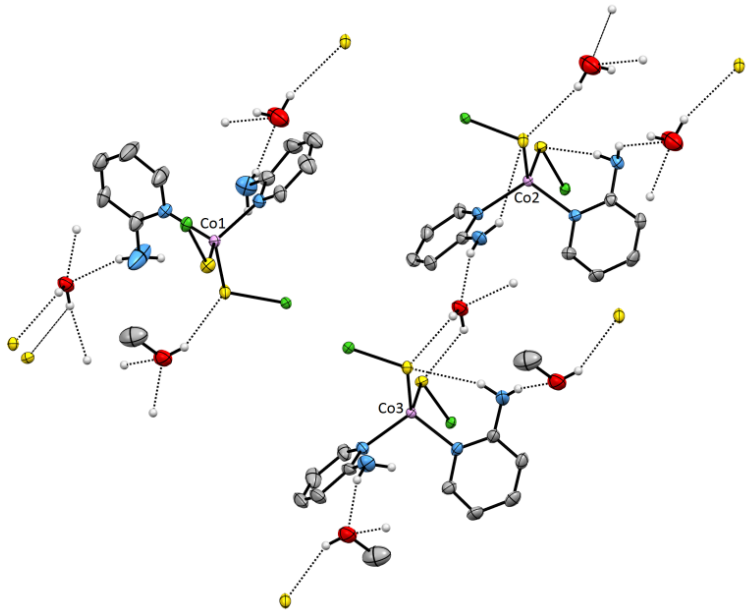

Fig. S2 The net of hydrogen bonding interactions between molecules of compound **1** (S-yellow, O-red, N-blue, Si-green, Co-pink, C – grey, H-white).

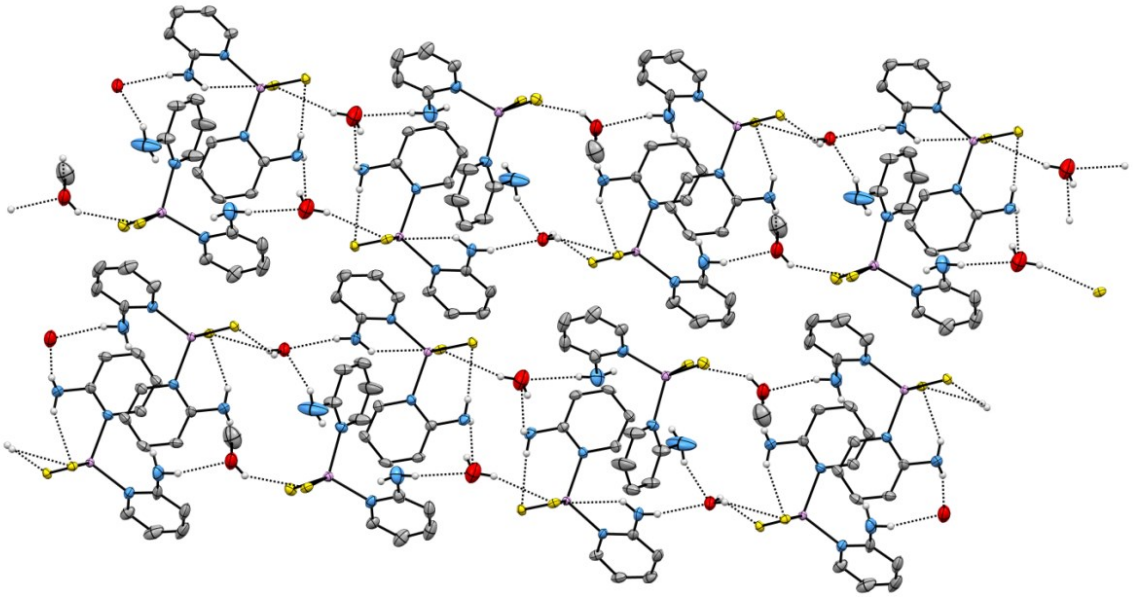

Fig. S3 The crystal packing of **1** along *b* axis with hydrogen bonding interactions shown as dashed lines. H atoms and *t*Bu groups omitted for clarity (S-yellow, O-red, N-blue, Si-green, Co-pink, C-grey).

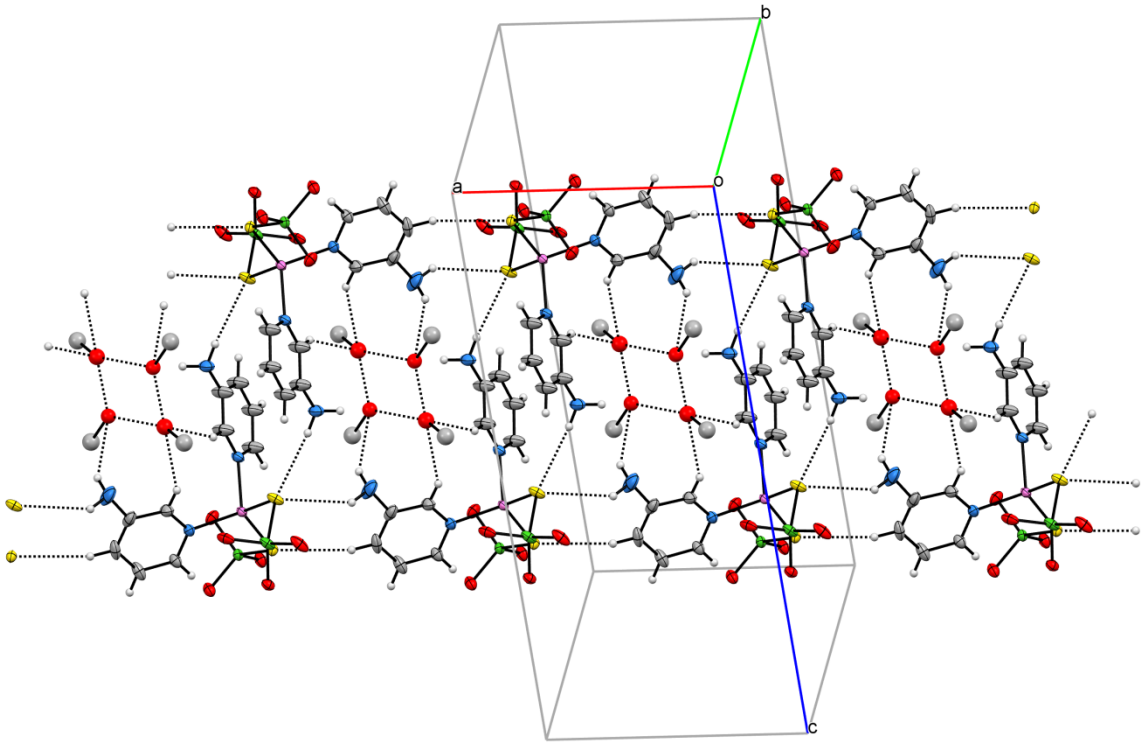

Fig. S4 The view on the polymeric chain of compound **2** with hydrogen bonding interactions shown as dashed lines. *t*BuO groups omitted for clarity (S-yellow, O-red, N-blue, Si-green, Ni-celadon, C - grey).

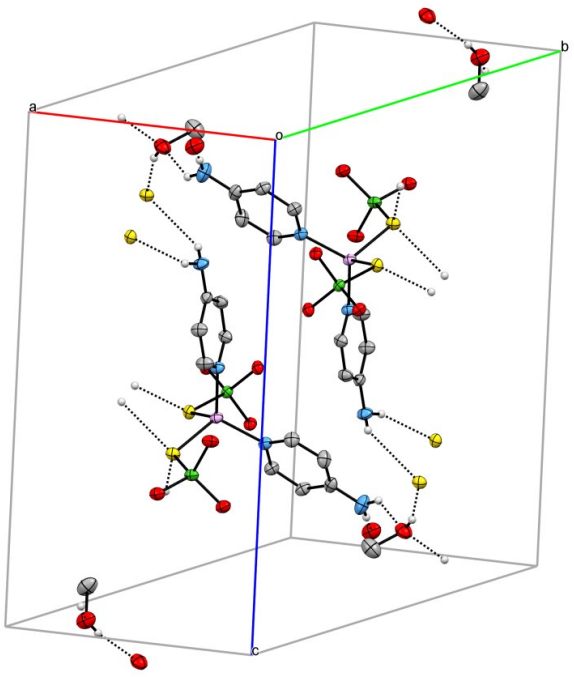

Fig. S5 The net of hydrogen bonding interactions between molecules of compound **3** (S-yellow, O-red, N-blue, Si-green, Co-pink, C – grey, H-white).

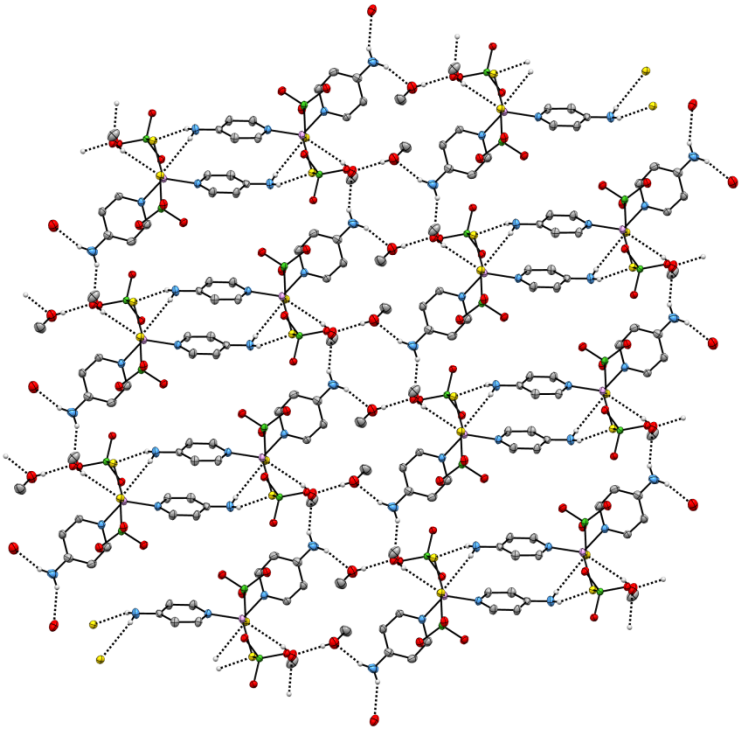

Fig. S6 The crystal packing of **3** along *a* axis. with the hydrogen bonding interactions shown as dashed lines. tBu groups omitted for clarity (S-yellow, O-red, N-blue, Si-green, Co-pink, C - grey).

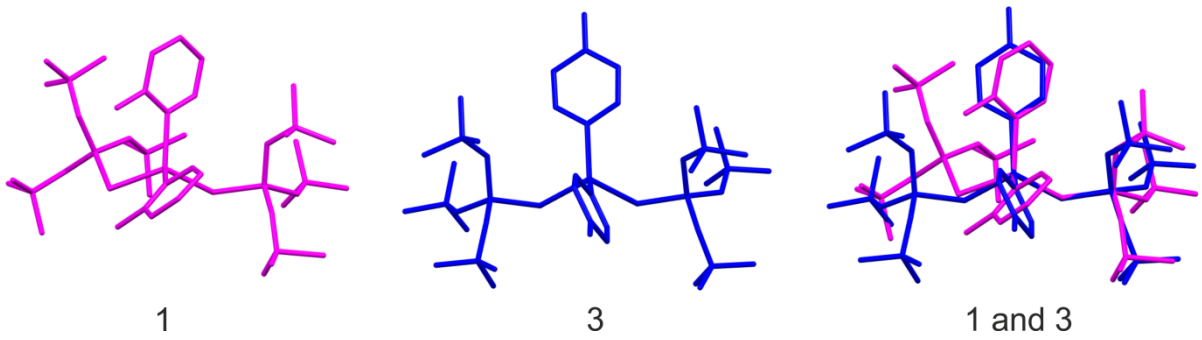

Fig. S7 The overlay of X-ray molecular structures of complexes **1** and **3** generated by superimposing the coordination centers (Co, N, S atoms).

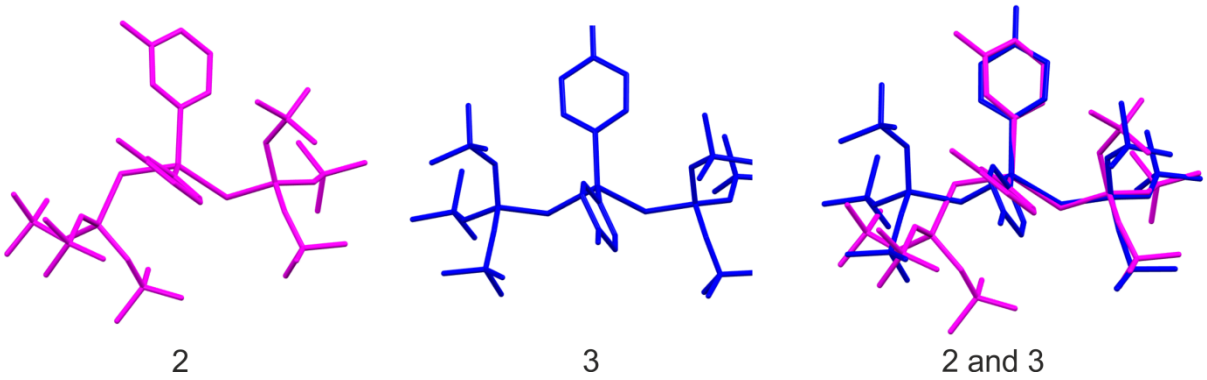

Fig. S8 The overlay of X-ray molecular structures of complexes **2** and **3** generated by superimposing the coordination centers (Co, N, S atoms).

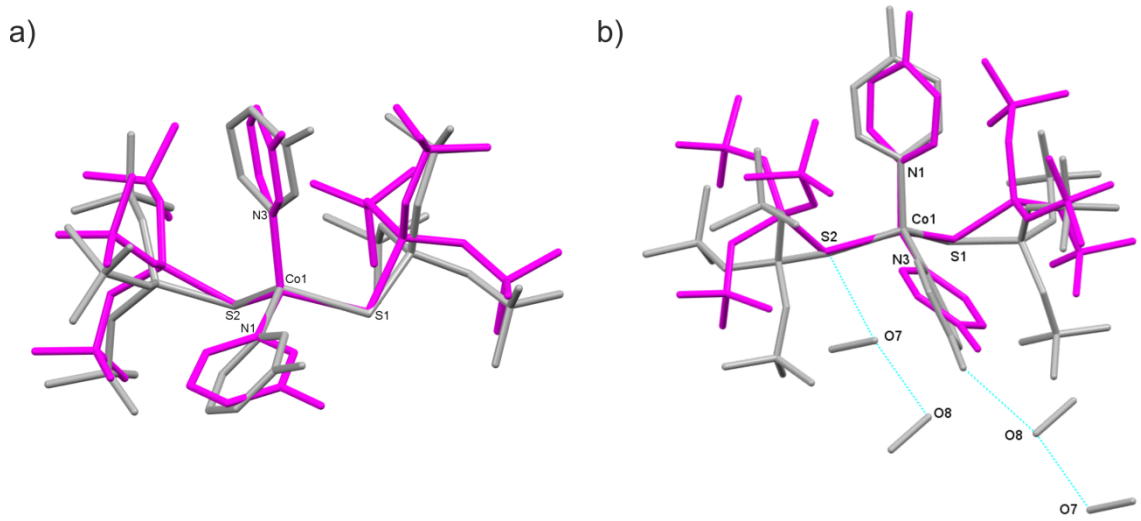

Fig. S9 The overlays of calculated (magenta) and X-ray (grey) molecular structures of: a) complex **2** and b) complex **3**. Overlays were generated by superimposing the coordination centers (Co, N, S atoms).

Figure S9 a) and b) presents an overlay of calculated and experimental structures of complex **2** and complex **3**. The number of the unpaired electrons of the central cobalt(II) ion was correctly assigned as **3** since the overall geometry of the metal center did not change as a result of geometry optimization and remained tetrahedral. The observed rotation of the silyl substituents in **3** results obviously from the lack of intermolecular interactions – calculations were performed for vacuum and solvating molecules of methanol were removed from the structure of **3** before optimization procedure.

The shapes and energies of singly occupied HOMO and LUMO orbitals illustrated in Fig. S10 differ substantially for **2** and **3** which explains the differences between the absorption spectra of these compounds. Contrary to complexes **1** and **2** molecules of **3** exhibit approximate C_{2v} symmetry, which is reflected in the shape of its molecular orbitals as well as position and intensity of its absorption bands. Calculated UV-Vis spectra of **2** and **3** (including the first 300 excitations) are illustrated in Fig. S16.

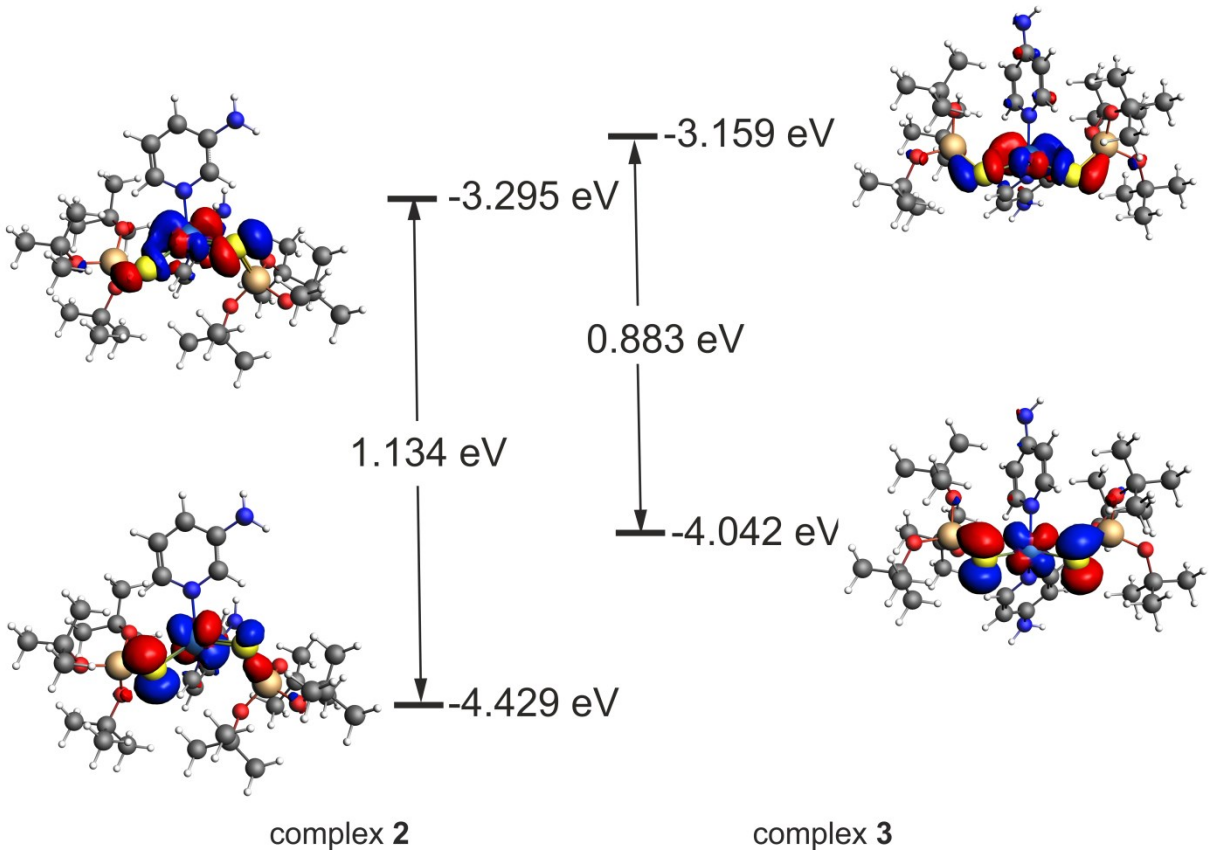

Fig. S10 The illustration of energies and shapes of singly occupied HOMO and LUMO orbitals of complexes **2** and **3** calculated at BP86-D/TZP level.

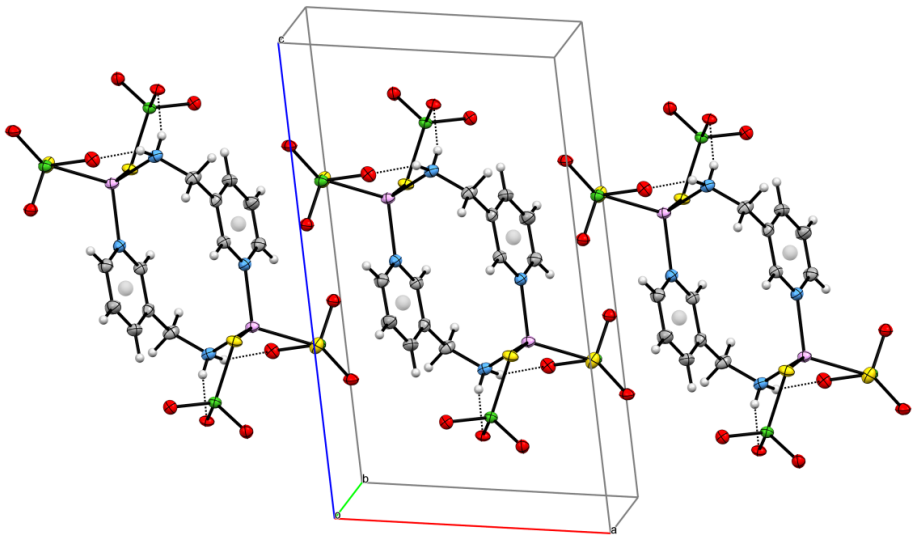

Fig. S11 The crystal packing of **4** along *b* axis with the hydrogen bonding interactions shown as dashed lines. tBu groups omitted for clarity (S-yellow, O-red, N-blue, Si-green, Co-pink, C - grey).

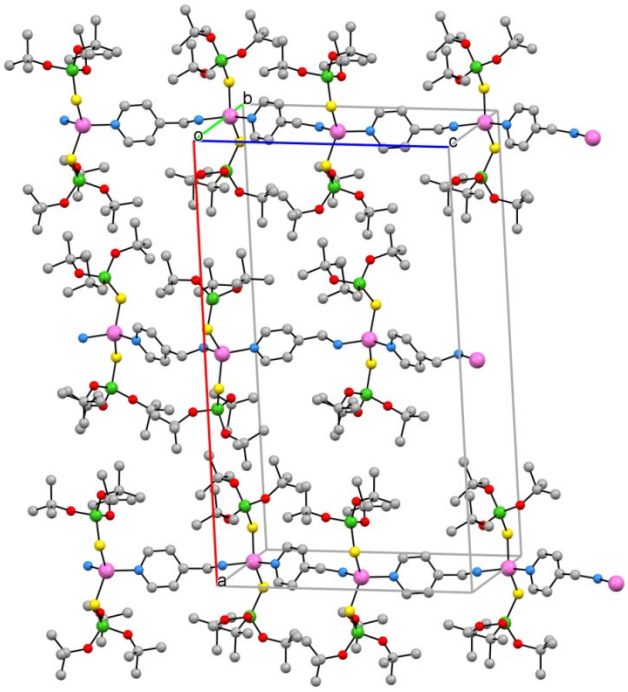

Fig. S12 The crystal packing of **5** along *b* axis with the hydrogen bonding interactions shown as dashed lines. H atoms omitted for clarity (S-yellow, O-red, N-blue, Si-green, Co-pink, C - grey).

The FTIR spectrum of complex **1** shows the presence of sharp band located at 3612 cm^{-1} which confirms the presence of water molecules in the structure of the compound. Although the most distinctive vibrational characteristic of H_2O molecule usually is the broad asymmetric spectrum about 3400 cm^{-1}, but when the molecule is isolated in hydrophobic surrounding it exhibits the O–H vibrations as a sharp band located in the range of 3700-3580 cm^{-1}. The similar trait was previously observed at 3664 cm^{-1} in the FTIR spectrum of sodium aryloxysilanethiolate [Na{SSi(Odipp)$_3$}(diglyme)(H_2O)] as the vibrations of isolated water molecule [S. Godlewska, K. Baranowska, A. Dołęga, *Inorg. Chem. Commun.*, 2014, **40**, 69; A. Jabłońska, J. Bender, D. Gudat, Ł. Ponikiewski, A. Dołęga, *Polyhedron*, 2016, **115**, 219]. Therefore, the O–H stretch band in complex **1** is reasonably shifted towards lower energy as a result of its engagement in the formation of intermolecular O–H_{water}···$S_{silanethiolate}$ hydrogen bonding interactions.

The crystal structures of complexes **1**-**3** exhibit the presence of methanol molecules verified in the FTIR spectrum by the presence of the stretching vibrations of the O–H in the range of 3480-3420 cm^{-1} which are also shifted due to their participation in the formation of hydrogen bonging interactions. The valence vibrations of amine N–H group are identified by the bands in the range of 3325-3140 cm^{-1} and they are shifted due to their particular participation in the formation of diverse hydrogen bond interactions like intermolecular N–H···O_{water} and N–H···$O_{methanol}$ in **1**, N–H···$S_{silanethiolate}$ in **2**, intermolecular N–H···$O_{methanol}$ and N–H···$S_{silanethiolate}$ in **3** and intramolecular interactions N–H···$O_{silanethiolate}$ in **4** and **5**.

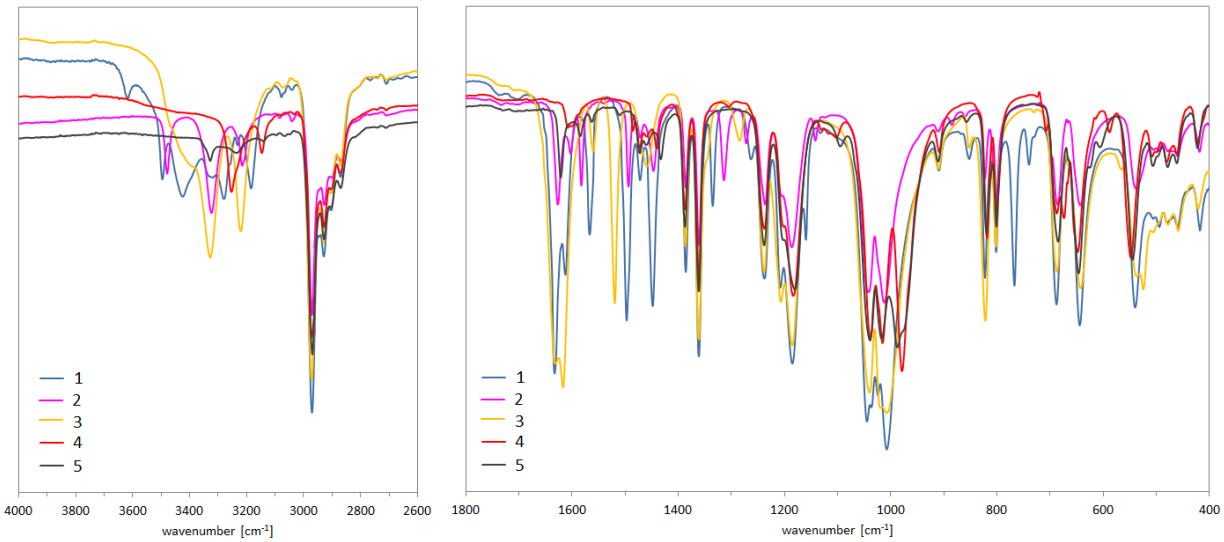

Fig. S13 FTIR spectrum of complex **1-5** in the range of 4000-400 cm^{-1}

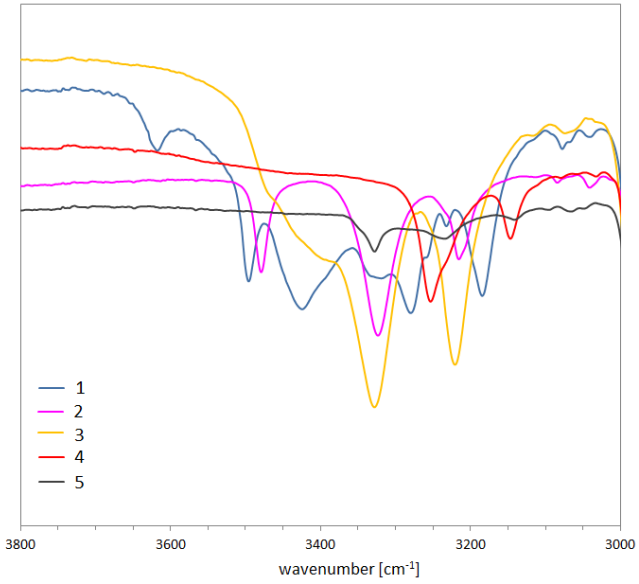

Fig. S14 FTIR spectrum of complex **1-5** in the range of 4000-3000 cm^{-1}.

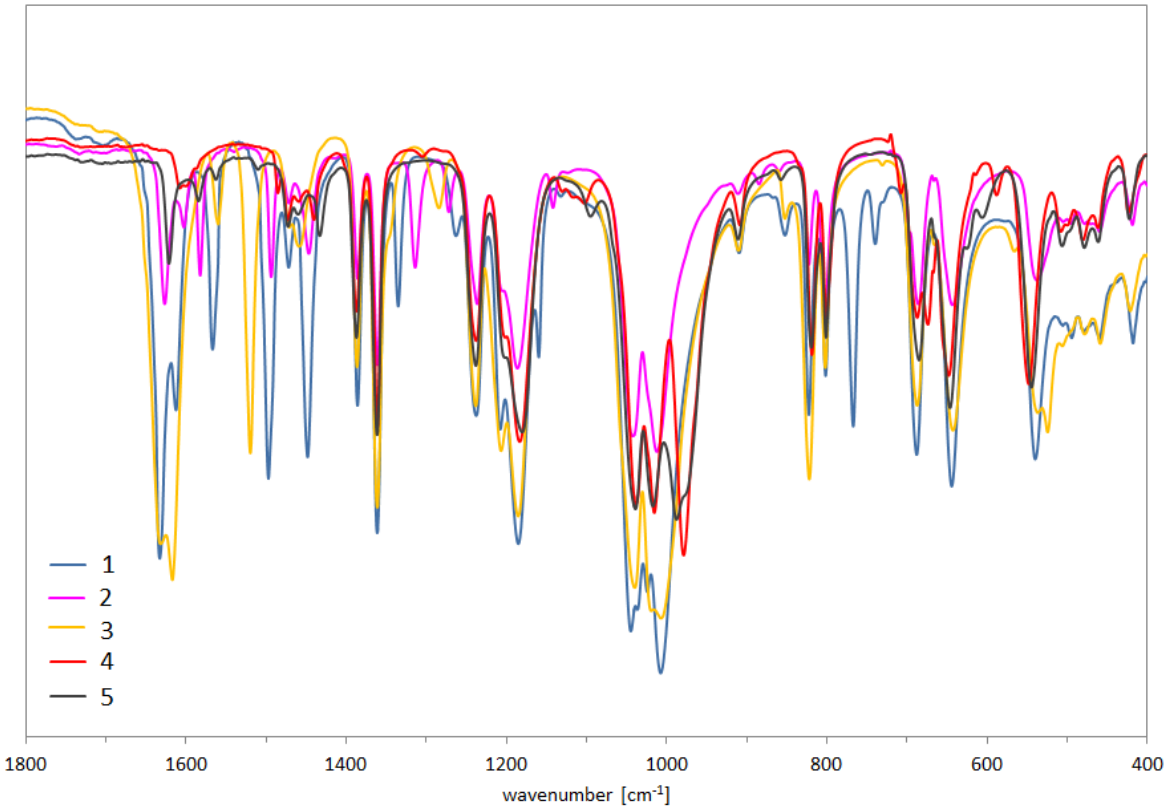

Fig. S15 FTIR spectrum of complex **1-5** in the range of 1800-400 cm^{-1}.

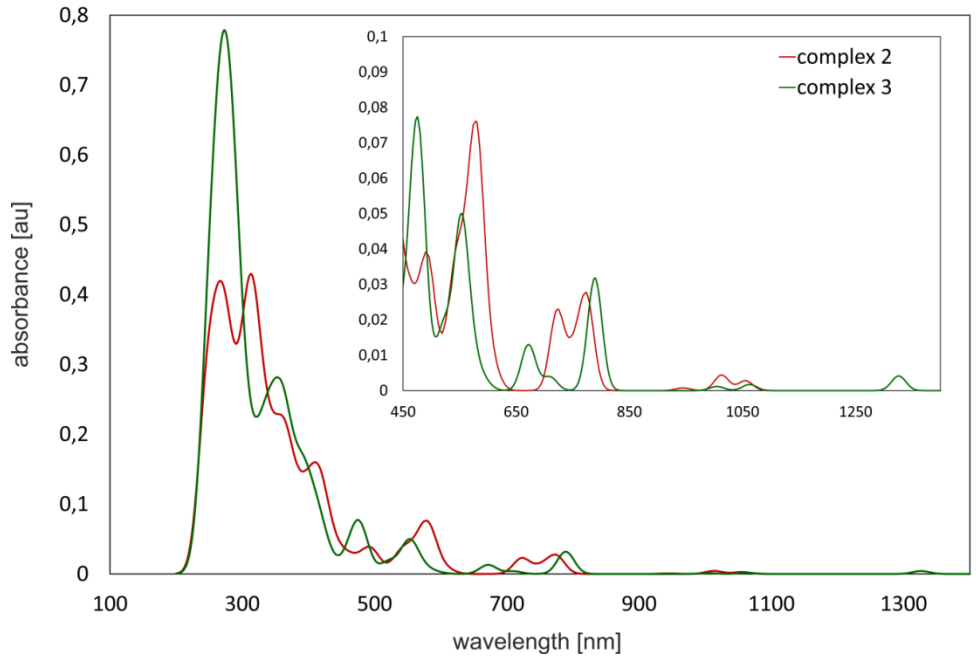

Fig. S16 A comparison of TD-DFT UV-Vis spectra of **2** and **3**.

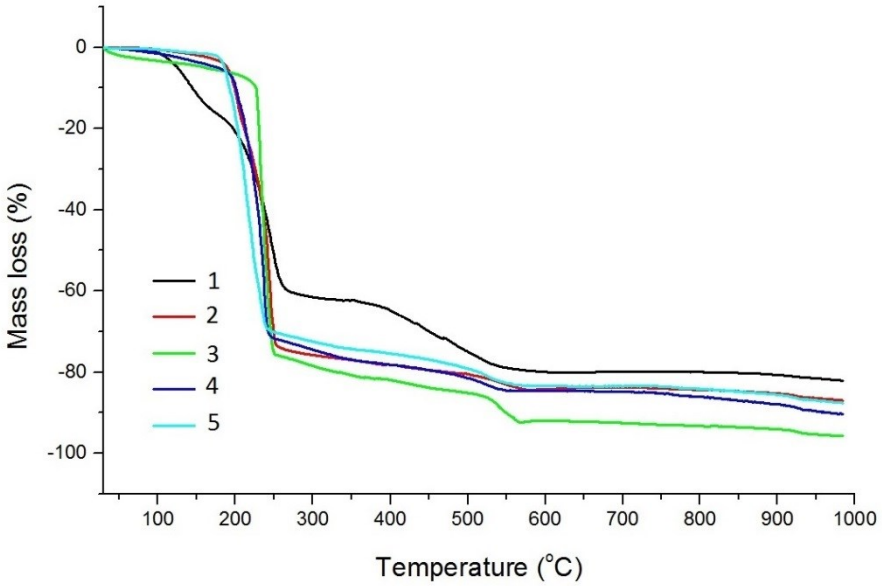

Fig. S17 Thermal decomposition of complexes **1-5** in air.

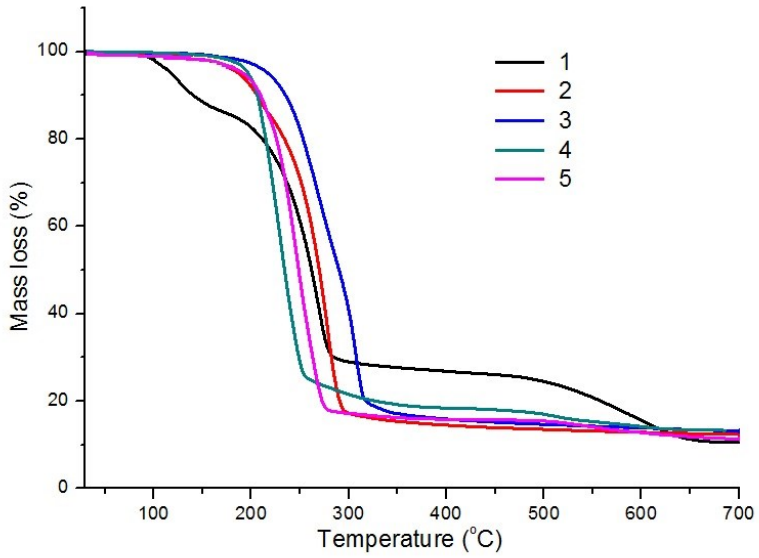

Fig. S18 TG curves of complexes **1-5** recorded in nitrogen atmosphere.

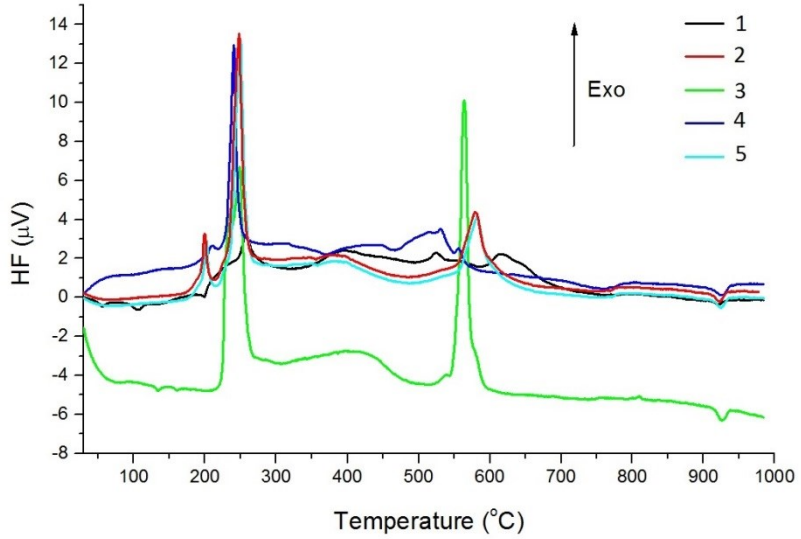

Fig. S19 DSC curves of complexes **1-5** recorded in air atmosphere.

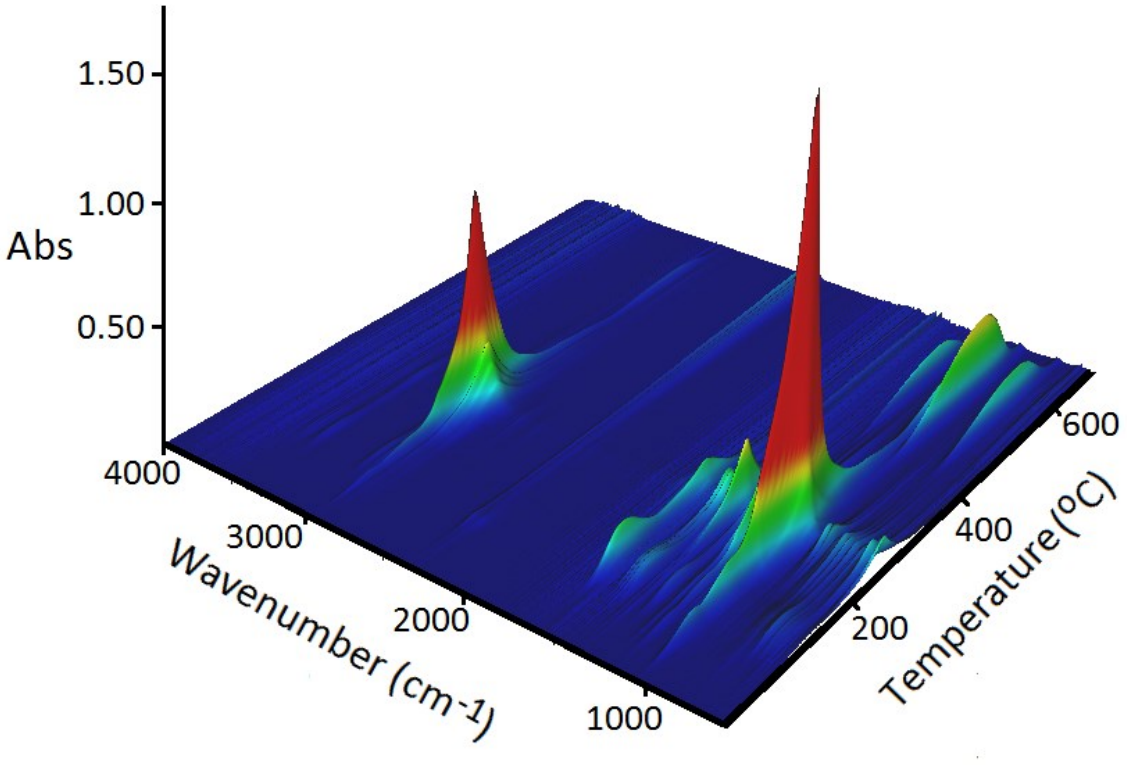

Fig. S20 Stacked plot of the FTIR spectra of the evolved gases for complex **1**.

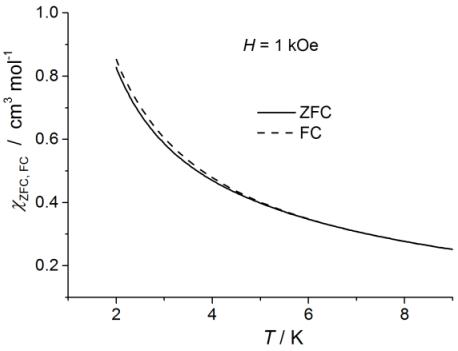

Fig. S21 Temperature dependences of χ_{ZFC} and χ_{FC} molar magnetic susceptibilities of **2** measured under 1 kOe *dc* magnetic field.

(a)

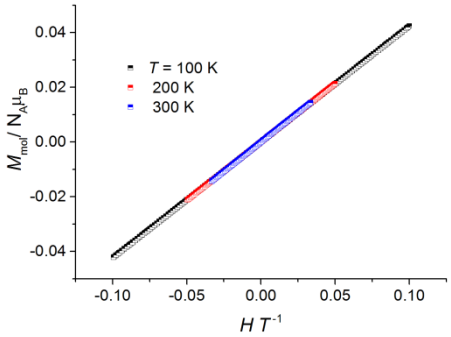

(b)

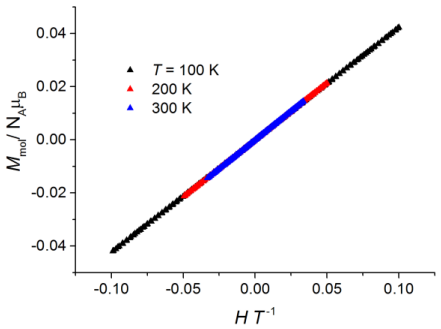

(c)

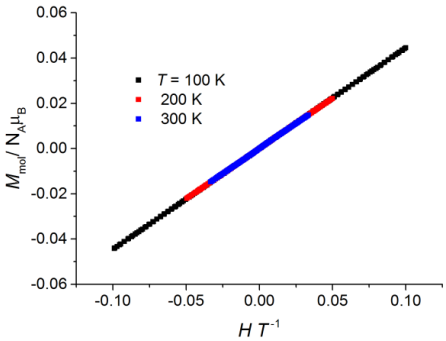

(d)

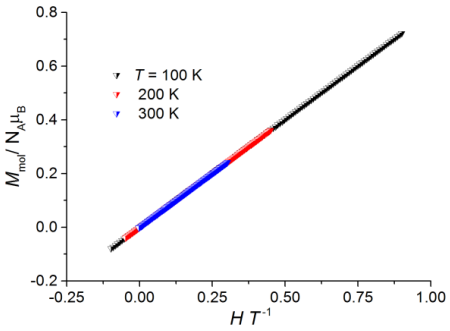

(e)

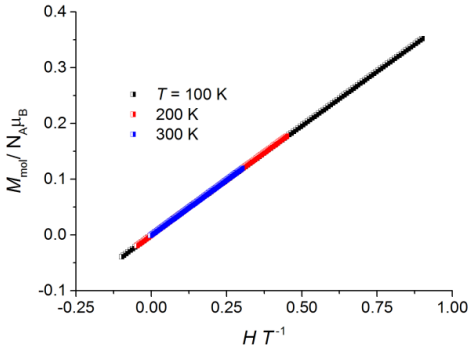

Fig. S22 Magnetization curves in reduced coordinates $M_{mol}/\mu_B N_A$ *vs* H/T, for **1** (a), **2** (b), **3** (c), **4** (d) and **5** (e), measured at 100, 200 and 298 K.

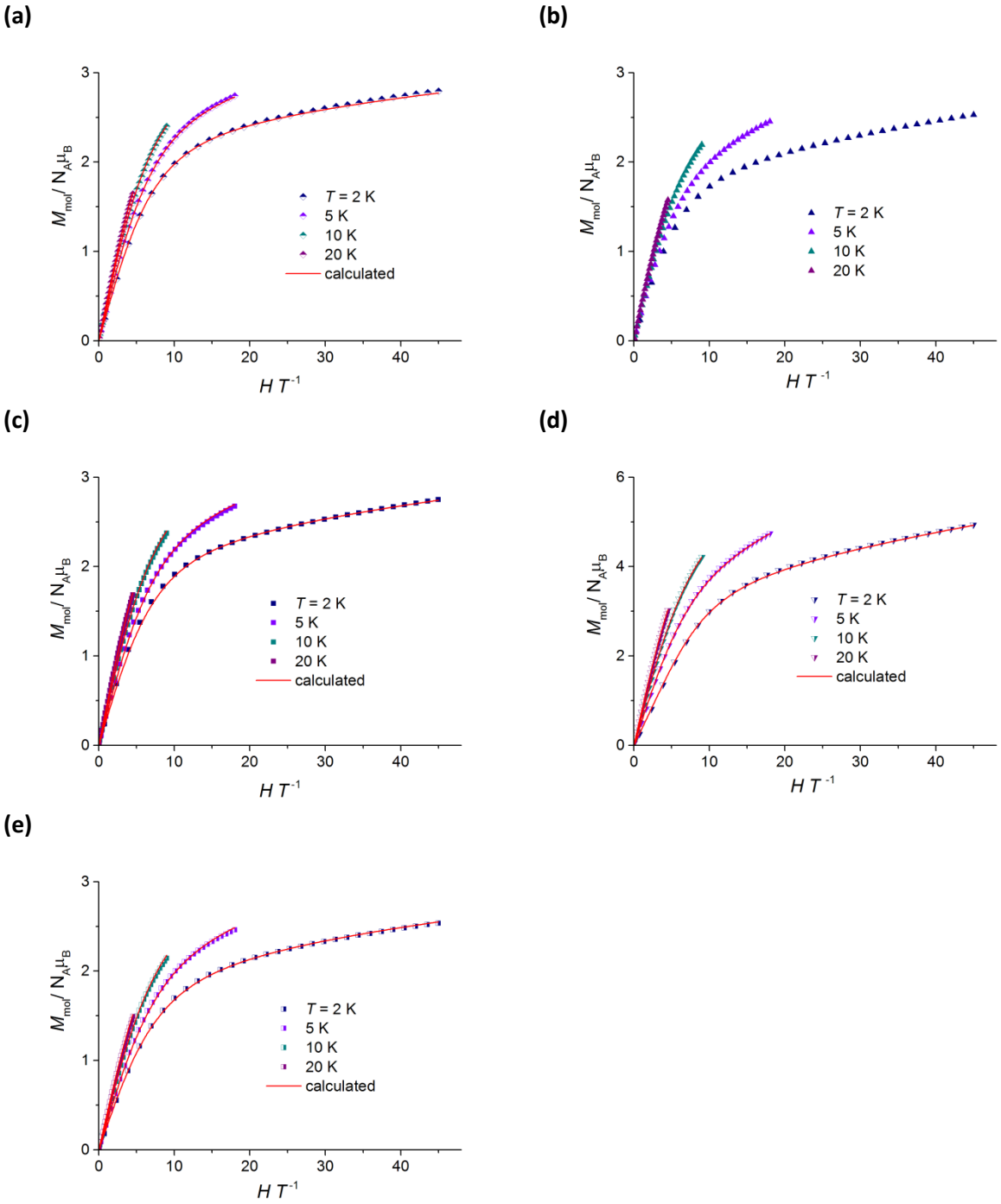

Fig. S23 Magnetization curves in reduced coordinates $M_{mol}/\mu_B N_A$ *vs* H/T, for **1** (a), **2** (b), **3** (c), **4** (d) and **5** (e), measured at 2, 5, 10 and 20 K (*symbols*). The solid red lines represent the best simulations of magnetic data for parameters presented in **Table 3** (see main text for details).

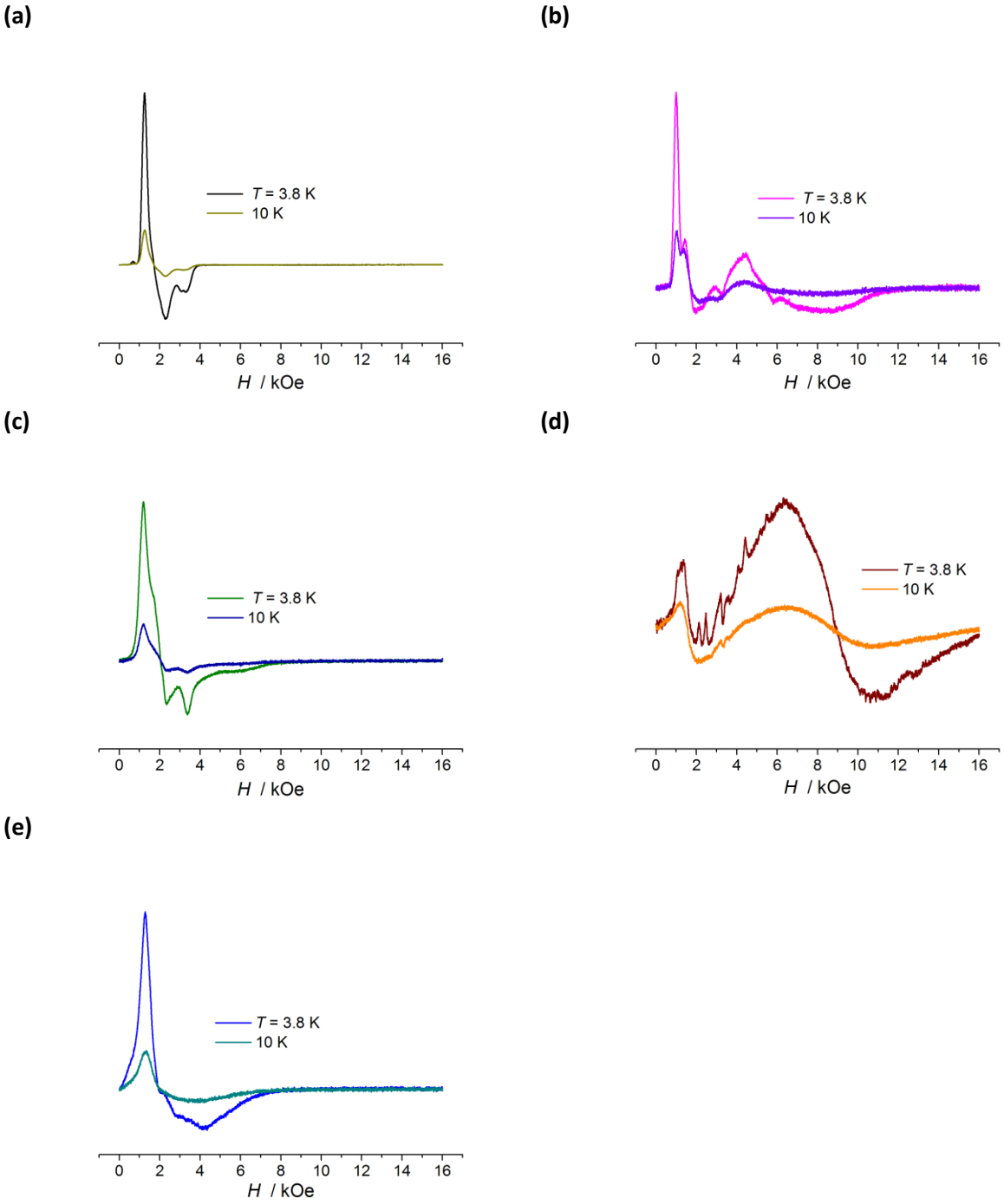

Fig. S24 Experimental X-band EPR powder spectra of samples **1** (a), **2** (b), **3** (c), **4** (d) and **5** (e), recorded at 3.8 and 10 K.

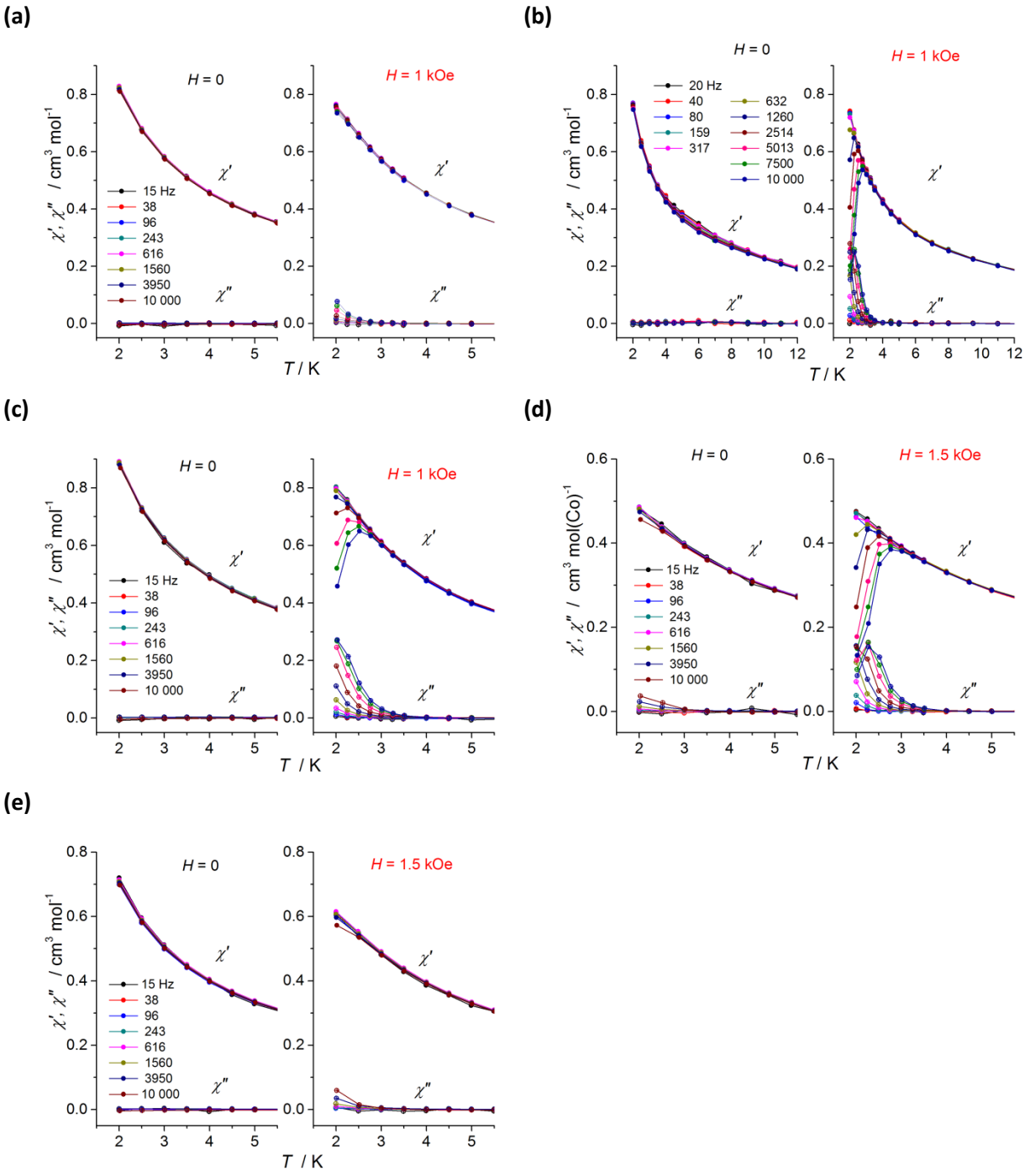

Fig. S25 Temperature dependences of variable-frequency in-phase χ' and out-of-phase χ'' *ac* susceptibility data, for **1** (a), **2** (b), **3** (c), **4** (d) and **5** (e) in the absence and presence of the static magnetic field (*ac* field frequencies selected from 15 Hz – 10 kHz range). For **4** the presented data are given per mole of Co(II) ions.

For **2,** the emergence of a slight χ' dependence on frequency in the temperature range ~4 < *T* < 10 K, without external magnetic field, may indicate weak inter-molecular FM coupling that was revealed by the *dc* variable-temperature measurements (see main text). In magnetic field, χ' becomes

frequency-independent above ~4 K, while below ~4 K, the field-induced slow magnetization dynamic, occurs. This effect is also illustrated in Fig. S28 by $\chi' T$ vs T dependencies measured at H = 0 kOe and H = 0.7 kOe. Notable is that, for **2**, the low temperature values of molar in-phase *ac* susceptibility component χ', as well as χ and M_{9T}, extracted from *dc* measurements, are comparable to their counterparts observed for other mononuclear compounds **1** and **3**. It suggests that in **2**, besides the main fraction of magnetically isolated Co(II) ions exhibiting field-induced slow magnetic relaxations, an admixture fraction of magnetically coupled cobalt centers exists. We suppose that the formation of such fraction of magnetically coupled cobalt ions in **2** may be induced by the loss of methanol solvent molecules - lack of solvent molecules, e.g. in the surface layers of crystallites, can lead to some disorders in crystal packing allowing inter-molecular magnetic interactions. To check if the loss of incorporated solvent molecules occurs when the sample is exposed to a vacuum in the PPMS, the measurements of the powdered **2** immersed in eicosane (melting point 310 K) have been also performed. No significant difference in magnetic results for samples **2** with and without eicosane was observed. This indicates that such loss of methanol solvent molecules would rather happened during the powdering process required to be done before magnetic measurements.

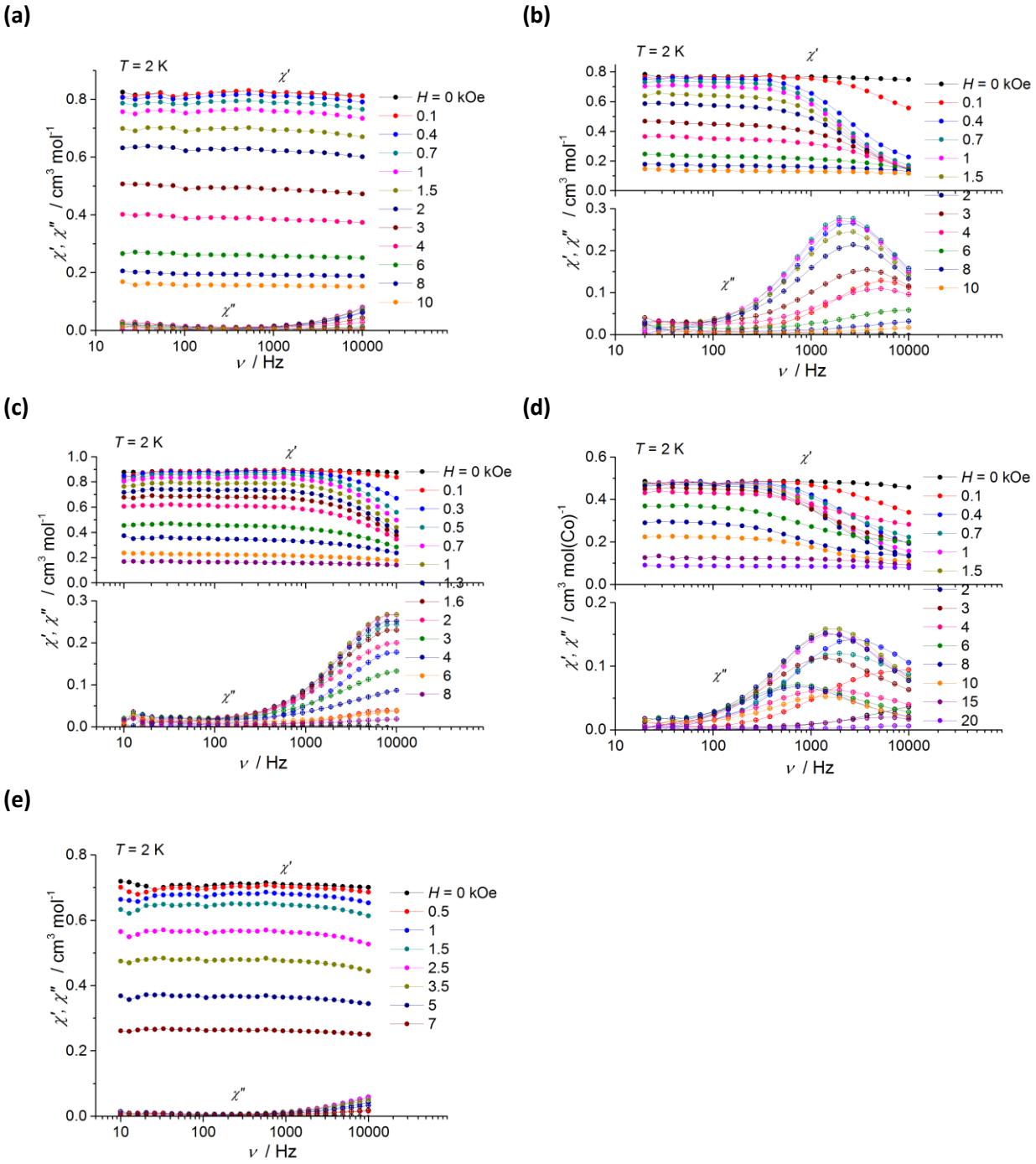

Fig. S26 Frequency-dependent in-phase χ' and out-of-phase χ'' *ac* susceptibility data, for **1** (a), **2** (b), **3** (c), **4** (d) and **5** (e), measured under different *dc* magnetic field, at 2 K (lines are guide to the eye). For **4** the presented data are given per mole of Co(II) ions.

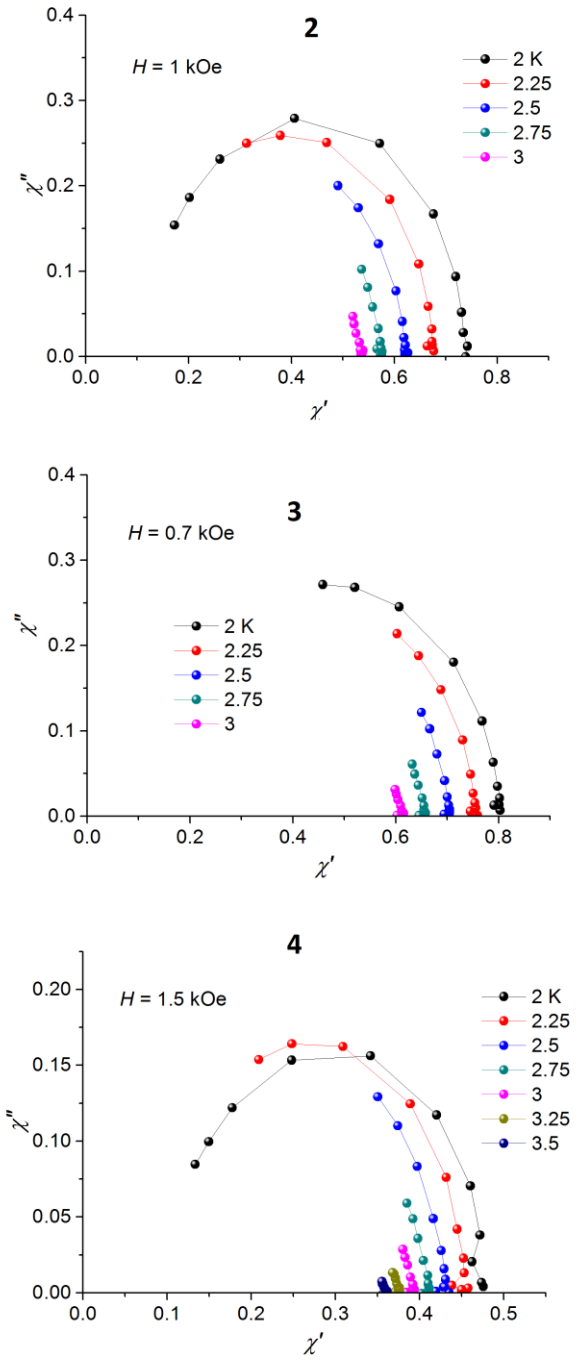

Fig. S27 Cole-Cole plots for **2** (upper), **3** (middle) and **4** (bottom) under optimum *dc* magnetic field, from 2 to 3.5 K (lines are guide to the eye). For **4** the presented data are given per mole of Co(II) ions.

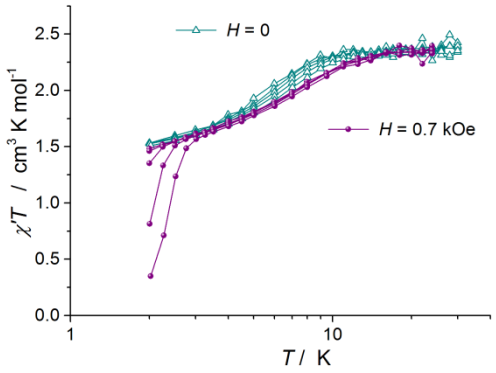

Fig. S28 Temperature dependences of variable-frequency *ac* susceptibility data $\chi' T$, for **2**, in the absence and presence of the static magnetic field.

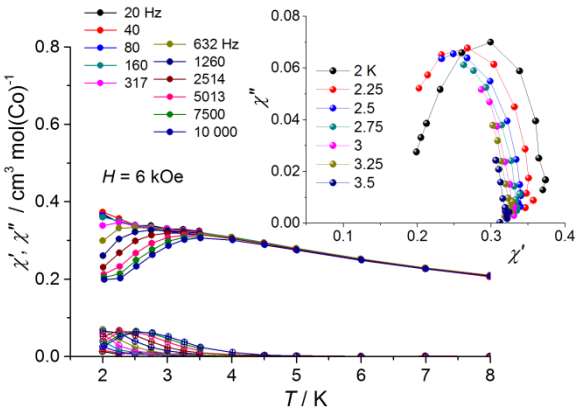

Fig. S29 Temperature dependences of variable-frequency *ac* susceptibility data, χ' and χ'', for **4** measured under 6 kOe *dc* field. Inset: Cole-Cole plot for **4** under 6 kOe *dc* field, from 2 to 3.5 K (lines are guide to the eye). Data are given per mole of Co(II) ions.

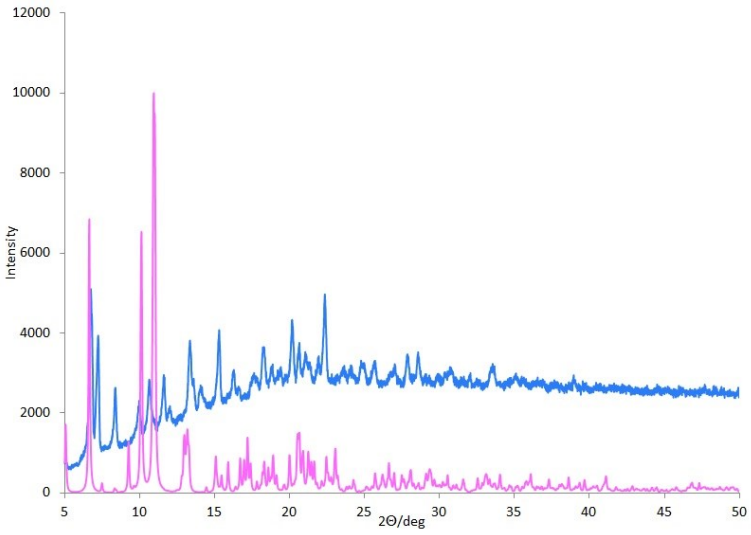

Fig. S30 The powder X-ray pattern of complex **1**: measured – blue line; the simulated pattern derived from single crystal data – pink line.

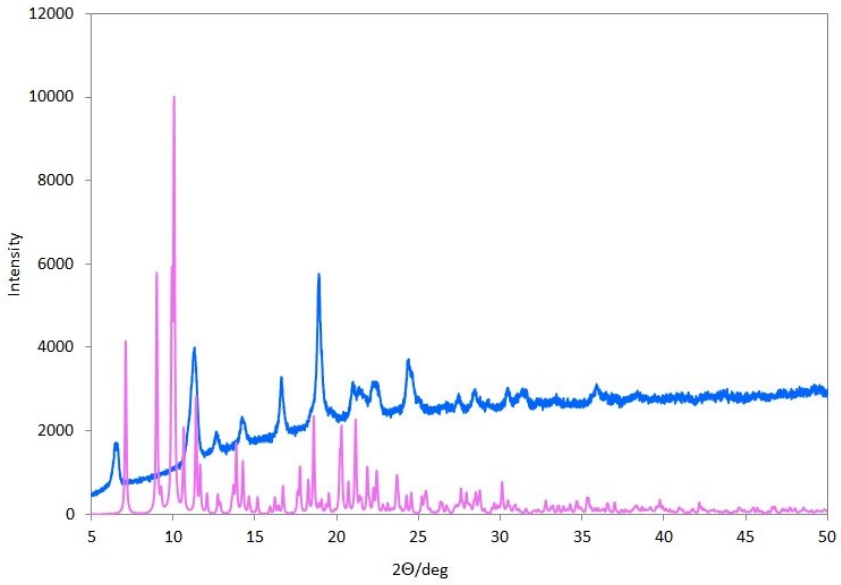

Fig. 31 The powder X-ray pattern of complex **2**: measured – blue line; the simulated pattern derived from single crystal data – pink line.

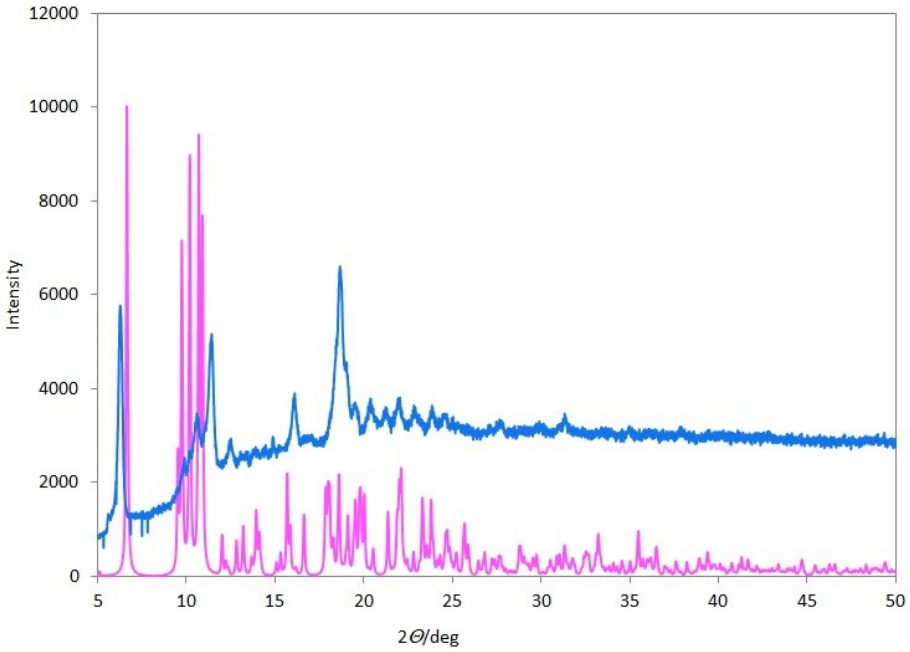

Fig. S32 The powder X-ray pattern of complex **3**: measured – blue line; the simulated pattern derived from single crystal data – pink line.

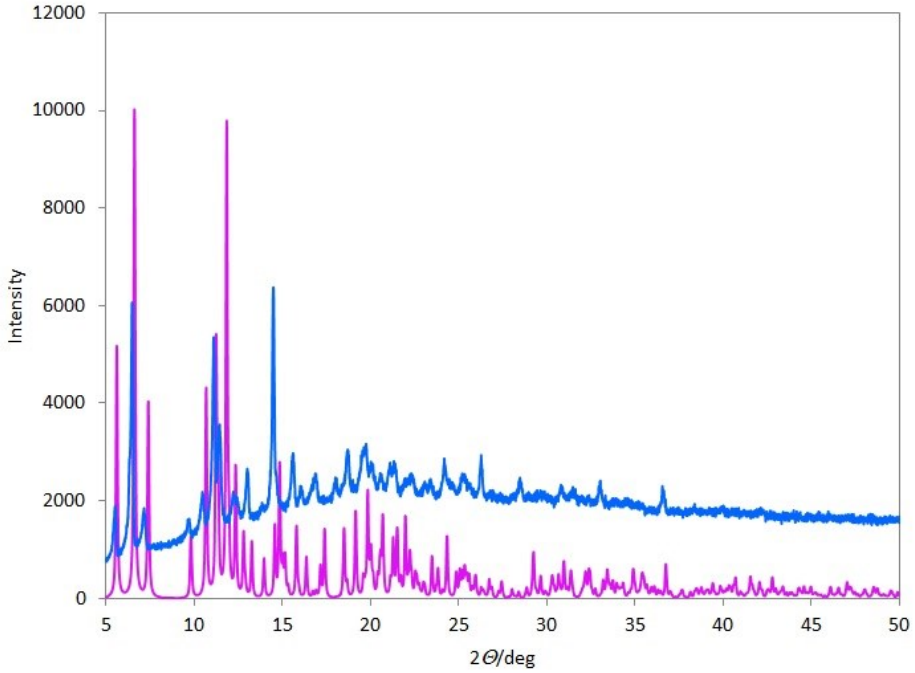

Fig. S33 The powder X-ray pattern of complex **4**: measured – blue line; the simulated pattern derived from single crystal data – pink line.

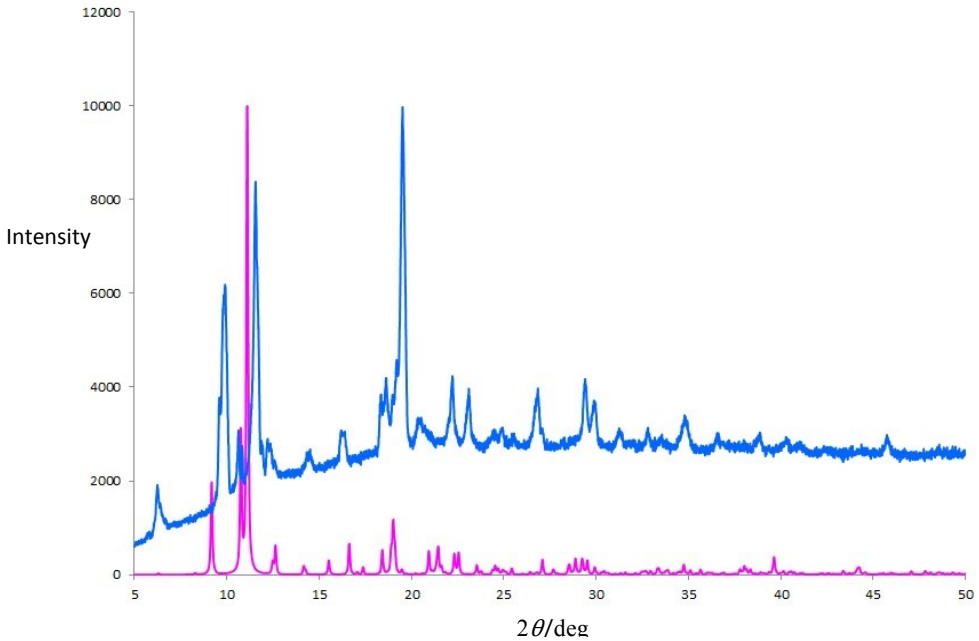

Fig. S34 The powder X-ray pattern of complex **5**: measured – blue line; the simulated pattern derived from single crystal data – pink line.